NUMERICAL CALCULATION OF IRON- AND PULSATION LOSSES ON INDUCTION MACHINES WITH OPEN STATOR SLOTS

JJ Germishuizen*, A Jöckel* and MJ Kamper**

*Siemens Automation and Drives, Germany, **University of Stellenbosch, South Africa.

Abstract. Pulsation losses, which are very difficult to measure, are present in every squirrel cage induction motor and depend mainly on the geometrical design. This paper primarily deals with the question whether these losses can be calculated by means of numerical methods. For this purpose two induction motors that only differ in the slot design are measured at no- and full-load and compared with the computed results.

Key Words. Iron losses, Pulsation losses, Eddy currents, Induction motor, Loss separation

1. INTRODUCTION

In this paper two induction motors with open stator slots in the 200 kW range are used to investigate the numerical calculation of iron- and pulsation losses. The motors used have the same outer dimensions and will be referred to as motor A and B. The main differences are the slot designs. Motor A and B, have 60 and 36 stator slots respectively, have different rotor leakage slots and have 40 and 36 number of series turns respectively. For the study the measurements are performed at 50 Hz.

The no-load loss consists of the iron losses and the eddy-current losses arising from changing flux densities in the iron of the machine with only the stator winding energized. A more or less large part of these losses occur already under no-load condition and is measured in the no-load test. Especially the eddy-current losses are difficult to calculate analytically and are quite often estimated as more or less lump-sum additions to the iron losses in the iron loss calculations [1], [2].

1.1 Pulsation losses

In general the discontinuities in magnetic field components as rotor teeth and slots sweep past the stator and the rotating stator field produce loss in both the stator and rotor laminations that isn't accounted for by the hysteresis and dynamic loss in the steel [3]. Flux pulsations in the rotor teeth for example will cause eddy-currents in the rotor bars, even at no-load. These additional eddy-current loss is the focus of the paper and is referred to as pulsation loss.

1.2 No-load losses

The no-load test on an induction machine gives information with respect to the exciting current and no-load losses. At no-load only a very small value of rotor current is needed to produce sufficient torque to overcome friction and windage. The rotor copper losses are therefore usually assumed to be negligibly small while the stator copper losses may be appreciable because of the larger exciting current. The core loss are usually confined largely to the stator iron. Therefore the input power can be approximated as

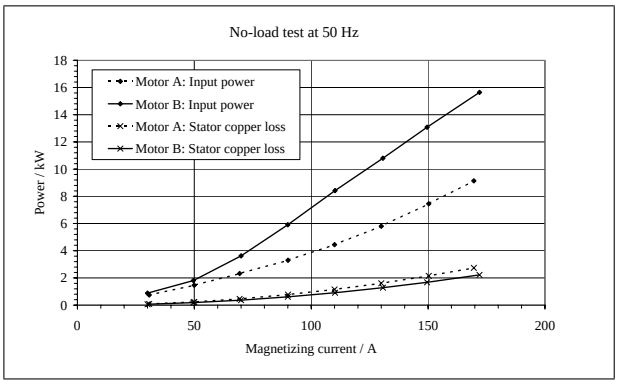

Fig. 1: No-load test results for motor A and B at 50 Hz.

$$\begin{aligned} P_{input} &= P_f + P_{Cu} + P_{Fe} \\ &= P_f + P_{Cu_1} + P_{Cu_2} + P_{Fe_1} + P_{Fe_2} \\ &\approx P_f + P_{Cu_1} + P_{Fe_1} \end{aligned} \quad (1)$$

where P_f is the friction and windage losses. The no-load losses at 50 Hz for the two induction motors are shown in Fig. 1. At 110 A magnetizing current motor B has approximately 2,5 kW more no-load losses than motor A. Since the tests for both motors are performed at 50 Hz the friction and windage losses will be the same. The stator copper losses are similar and from Eq. (1) the motors then only differ in the stator no-load loss. Thus, the increase in losses is added to the stator core loss. In this case it is questionable if the flux pulsations can cause this amount of extra losses at no-load and magnetizing current.

1.3 Full-load losses

The results from the no-load test are insufficient to determine the cause of the losses at a first instance. A heat-run test at 50 Hz will supply more information to find the cause of the increased losses. The results from the heat-run test are given in Table 1. From the heat-run test motor B has an efficiency of 89,5 % compared to the efficiency of 93,4 % of motor A. This is because motor B has much more total losses. The temperature rise in the rotor of 114 and 260 for motor A and B respectively implies that the cause for the extra losses will be in the rotor.

		Motor A	Motor B
f	Hz	50	50
P_{input}	kW	214,8	190,1
$P_f + P_{Fe}$	kW	3,7	10,1
P_{Cu_1}	kW	7,0	5,8
P_{Cu_2}	kW	2,5	3,1
$slip$		0,0124	0,0175
P_{total}	kW	14,2	19,9
η	%	93,4	89,5
ΔT_{Stator}	K	114	161
ΔT_{Rotor}	K	114	260

Table 1: Heat-run test at 50 Hz.

2. LOSS CALCULATION

The losses for the investigation are calculated numerically using the Maxwell 2D transient solver from Ansoft and the focus will be on the total iron losses and rotor copper loss.

2.1 Iron losses

These losses are linked with the magnetization process and consists of three parts. The so-called separation of losses implies that the average power loss per unit volume of any material is decomposed into the sum of hysteresis and a dynamic contribution. For several alloys and sinusoidal excitation with a given frequency and magnetization the specific losses can be written as [5]

$$\begin{aligned} P_{W.kg^{-1}} &= P_{hyst} + P_{dyn} \\ &= P_{hyst} + P_{class} + P_{exe} \\ &= k_h B^2 f + k_c (Bf)^2 + k_e (Bf)^{1,5} \end{aligned} \quad (2)$$

In case of a lamination of thickness d and in the range of magnetizing frequencies where the skin effect is negligible the classical eddy-current loss has the form

$$P_{class} = \frac{(\pi\sigma)^2 d}{6} (Bf)^2 \quad (3)$$

where σ is the electrical conductivity. Thus, the only unknowns in Eq. (2) to be determined are k_h and k_e. For a given magnetizing, B, and by defining the following constants

$$k_0 = k_h B^2 \quad (4)$$

$$k_1 = k_c B^2 \quad (5)$$

$$k_2 = k_e B^{1,5} \quad (6)$$

Eq. (2) can be rewritten as a function of the magnetizing frequency, f_m,

$$\frac{P}{f_m} = k_0 + k_1 f_m + k_2 \sqrt{f_m} \quad (7)$$

Eq. (7) can easily be solved by a least square method. From this the unknown constants in Eq. (2) can be determined. The coefficients for the specific losses only hold for unprocessed laminations. Thus, the increase in iron losses due to punching and current dependence are not accounted for in this way. Maxwell 2D provides a macro for calculating the iron losses by means of loss separation [4]. The calculation of iron losses still present difficulties and the search for improved methods continue [6], [7].

2.2 Rotor copper losses

The eddy-currents in the rotor arises from flux pulsations in the rotor teeth. These flux pulsations can be calculated by defining some dummy objects in the rotor teeth to simplify the calculation of the average flux densities. The average flux density in each of the rotor teeth at each time step of the transient analysis can then be calculated as

$$B_{tooth,avg} = \frac{1}{A} \int_A \left\| \overline{B} \right\| \, da \quad (8)$$

Once the flux density in each tooth as a time function is known a Fourier analysis is used to determine the DC-flux component as well as the higher order harmonics under no-load. The differential flux densities between two adjacent rotor teeth will be an indication of the flux pulsation seen by the rotor bar between the teeth.

Using a 2D finite element model the rotor currents only have a component in the z-direction. Similar to the average flux density in a tooth the loss of each rotor bar is calculated by means of a macro after each time step as

$$\begin{aligned} P_{Cu_2} &= R_2 \sum_1^n I_n^2 \\ &= R_2 \sum_1^n \int_{A_n} \left\| J_z \right\|^2 \, da \end{aligned} \quad (9)$$

where R_2 is the resistance of a rotor bar, n the total number of bars and A_n the cross-section area of a bar.

3. FINITE ELEMENT ANALYSIS

The Maxwell 2D transient solver is used to calculate the iron- and rotor copper losses as given in Eq. (2) and Eq. (9) respectively. For the iron losses, calculated by means of the separation of losses, a build-in macro is used which needs the coefficients k_h, k_c and k_e as input. These can be determined as explained in 2.1 or obtained from the manufacturer. The rotor copper losses are calculated using a user defined macro that performs the calculation given in Eq. (9). Due to the slot symmetry only a quarter, which is one pole, needs to be modeled.

$B_{tooth,avg}$ is also calculated using a user defined macro. Since the flux density is a vector having x- and y-components in a 2D FEA, the magnitude is averaged over a pre-defined area.

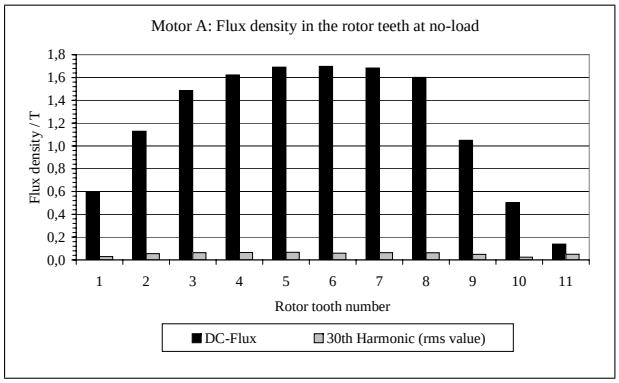

Fig. 2: Flux density in rotor teeth for motor A.

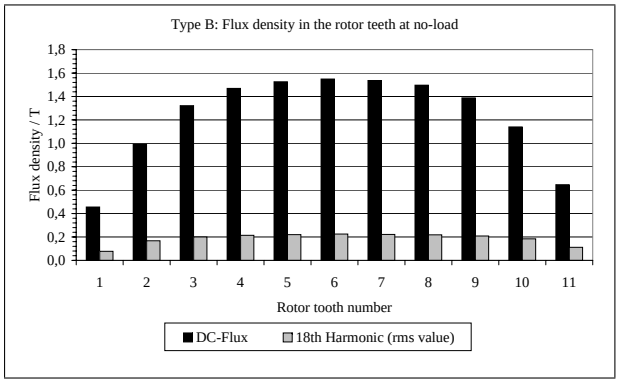

Fig. 3: Flux density in rotor teeth for motor B.

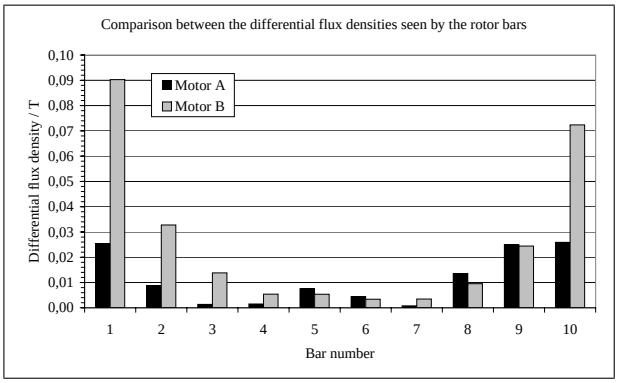

Fig. 4: Differential flux for the rotor bars.

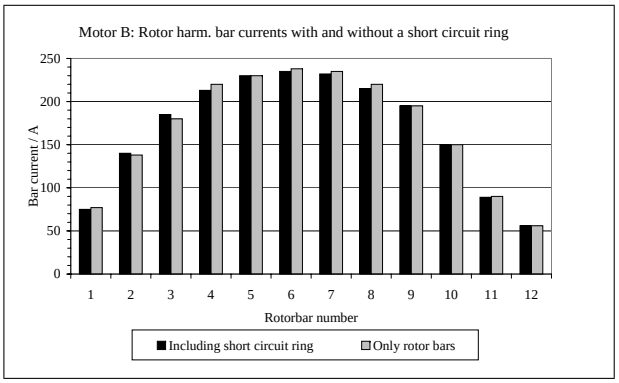

Fig. 5: Comparison with and without short circuit ring.

3.1 Average rotor tooth flux density

Figs. 2 and 3 shows the Fourier analysis of the rotor teeth flux densities for motor A and B respectively. Note the sinusoidal distribution of the flux densities over one pole. This confirms the sinusoidal distribution of the air-gap flux density. Due to the slot combinations the 30^{th} and 18^{th} slot harmonics are calculated for motors A and B respectively. For some teeth motor B has a harmonic amplitude of up to 3 times higher than calculated for motor A.

3.2 Differential flux densities

As explained in 2.2 the rotor copper losses arise from the flux pulsations in the rotor teeth. The differential flux densities of two adjacent rotor teeth will be an indication of flux pulsation seen by a rotor bar. Fig. 4 shows the differential flux densities. These already occur under no-load which means that currents will flow in each bar.

3.3 Eddy-currents in the rotor bars

The flux pulsations at no-load means eddy-currents and to proof this the rotor copper losses are calculated in a separate solution where the rotor short circuit rings are neglected. The only losses that can occur will be that of the eddy-currents. Neglecting the short circuit rings the results for the bar currents are shown Fig. 5. Note that this are the total bar currents and to get the eddy-current each bar current has to be divided by 2, thus

$$I_{eddy} = \frac{1}{2} \int_{A_n} \|J_z\|^2 \; da \tag{10}$$

This shows that even under no-load the rotor copper loss will be significant and in this case the cause for overheating. Fig. 6 shows a schematical representation of the eddy-currents in the bar.

3.4 Total FEA losses

The loss calculations for the two motors are now repeated using the methods as described in 2 for no-load. Table 2 shows the results of the loss calculations. Firstly notice the difference in the P_{Cu2} losses. Motor B has 2,7 kW due to eddy-currents and explain the temperature in the rotor during the

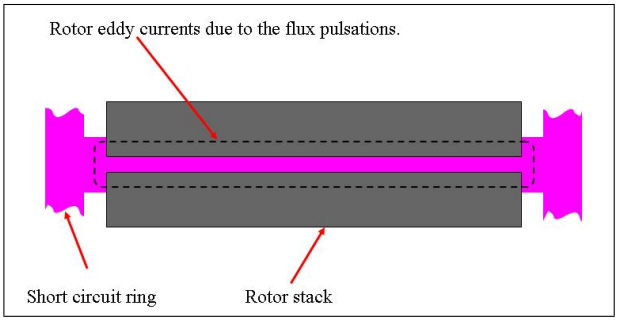

Fig. 6: Eddy-currents in the rotor bar.

		Motor A	Motor B
P_f	kW	0,3	0,3
P_{Cu_1}	kW	1,5	1,0
P_{Cu_2}	kW	0,6	2,7
P_{Fe}	kW	1,2	1,3
P_{total}	kW	3,6	5,3
$P_{measured}$	kW	4,4	8,2
ΔP_{loss}	$\%$	-18	-35

Table 2: FEA calculated losses.

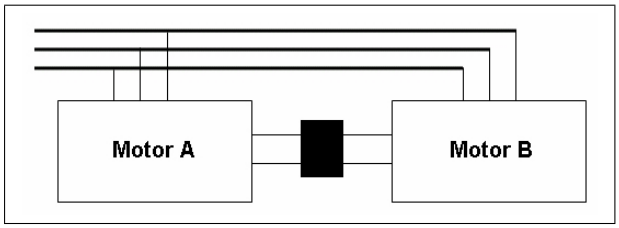

Fig. 7: Measurement setup of the coupled motors.

heat-run test. Comparing the P_{Fe} losses it differs by 0,1 kW. This results imply that the flux pulsations in motor B causes mainly rotor copper losses and that the increase in iron loss is small.

Comparing the total calculated losses with that measured there are still a difference of -18 % and -35 % for motors A and B respectively. The differences can be explained as follows:

1) The stator copper losses due to harmonics are neglected.
2) The coefficients for the iron losses are for unprocessed laminations and correction factors between 1,8 and 3,5 are reported for processed laminations [2].

This again shows care should be taken when measuring the no-load losses as given in Eq. (1) and assuming that no losses occur in the rotor. For a well designed motor this assumption holds. In the case of a poor design where flux pulsations causes no-load rotor copper losses this may lead to undesired overall results.

4. MEASUREMENTS

Measuring the no-load copper losses is very difficult. For that purpose a special measurement set-up has been used. The two motors were connected in parallel assuring that they both have the same supply voltage and frequency. Furthermore the two shafts were coupled using a coupling that allows the measurement of the shaft torque. The measurement set-up is shown in Fig. 7. The no-load tests were then repeated keeping motor A unchanged. Motor B has been changed in the following way in order to isolate the rotor copper losses. The following measurements were then taken:

1) both motors in coupled and in its original form
2) both short circuit rings of motor B were removed, thus having only the bars and
3) all the bars of motor B removed.

Fig. 8: Motor B with its cage removed.

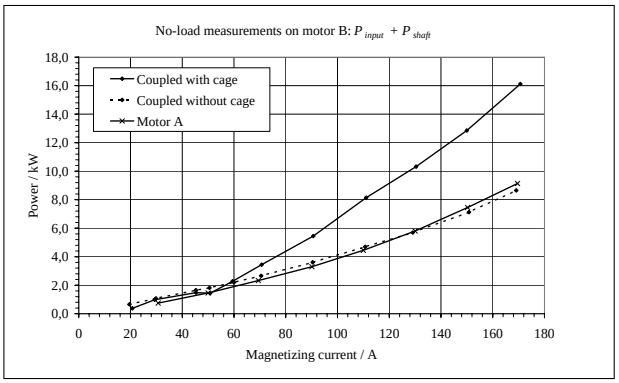

Fig. 9: No-load measured results for motor B.

The measurement with motor B having only the rotor bars showed that the input power is the same as with the short circuit rings. From this it is concluded that the eddy-currents will flow as shown in Fig. 6.

Fig. 8 shows motor B where the cage is removed. In the figure the stator end-winding can be seen as well. Just below the bottom part of the end-winding the empty rotor slots can be seen. With the motor coupled the sum of the measured input- and shaft power power as a function of the magnetizing current is shown in Fig. 5. For a reference the no-load losses of motor A in Fig. 1 is repeated. Without the cage the losses decrease to the same losses as was measured for motor A. The measurement thus confirm the calculation of the rotor copper losses as given in Table 2.

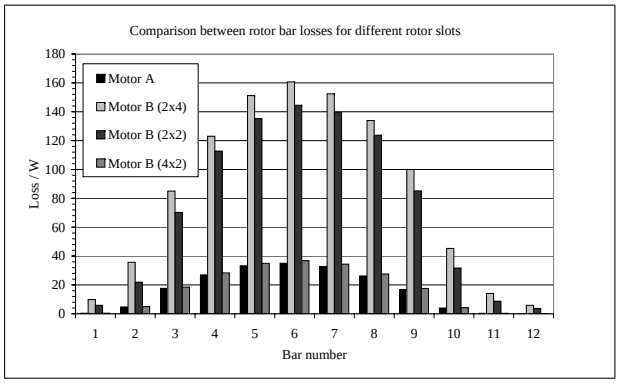

Fig. 10: Bar losses for different leakage slots.

5. DESIGN IMPROVEMENTS

The loss calculation methods are now used to compare different rotor leakage slot designs to reduce the rotor copper losses of motor B. For the comparison the bar losses of motor A are used as reference. The aim is to change the dimensions of the leakage slot in such a way as to achieve the same bar losses for motor B as was calculated for motor A. The leakage slot dimensions ($height \times width$) of motor B were changed in the following way:

1) 2 x 4 mm
2) 2 x 2 mm
3) 4 x 2 mm

The leakage slot of motor B is then varied to determine the effect of the leakage slot on the bar losses. The results are shown in Fig. 10. A leakage slot with the $height = 4\,mm$ and $width = 2\,mm$ results in almost the same losses as for motor A.

6. CONCLUSION

This paper has shown that the numerical calculation of iron- and pulsations losses can lead to design improvements. The measurement with the two motors coupled and the cage of motor B removed, as shown in Fig. 9, proofs that the rotor copper losses are the cause for the increased no-load losses for motor B. Furthermore it was shown that the changing flux densities have only a small influence on the iron losses. Special care should however be taken when calculating the iron losses by means of the separation of losses since the coefficients used are only valid for unprocessed laminations.

REFERENCES

[1] F. Taegen and R. Walezak, *Experimental verification of stray losses in cage induction motors under no-load, full-load and reverse rotation test conditions*, Archiv für Elektrotechnik 70 (1987) 255-263.

[2] K. Oberretl, *Eisenverluste, Flußpulsation und magnetische Nutkeile in Käfigläufermotoren*, Electrical Enigineering, 2000.

[3] R. L. Nailen, *Stray load loss: What's it all about*, Electrical Apparatus, August 1997.

[4] D. Lin, P. Zhou, W. N. Fu, Z. Badics and Z. J. Cendes, *A dynamic core loss model for soft ferromagnetic and power ferrite materials in transient finite element analysis*, Compumag 2003.

[5] G. Bertotti, *General properties of power losses in soft ferromagnetic materials*, IEEE Transactions on magnetics, Vol. 24, No. 1, January 1988.

[6] M. V. Ferreira da Luz, N. J. Batistela, N. Sadowski, R. Carlson and J. B. A. Bastos, *Calculation of iron losses in induction motors using finite element method*, ICEM 2000, 28-30 August 2000.

[7] G. Bertoti, A. Boglietti, M. Chiampi, D. Chiarabaglio, F. Fiorillo, and M. Lazzari, *An improved estimation of iron losses in rotating electrical machines*, IEEE Transactions on magnetics, Vol. 27, No. 6, November 1991.